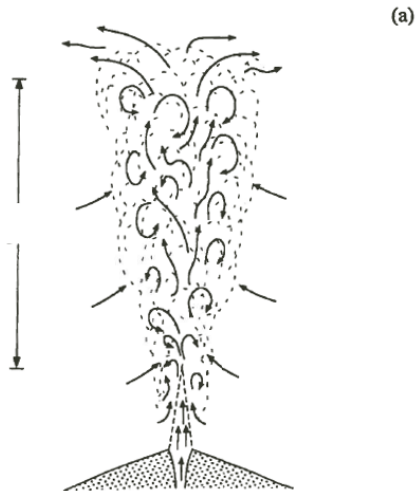**ERTH 456 / GEOL 556**
Volcanology

– Lecture 13: Volcanic Plumes II –

Ronni Grapenthin
rg@nmt.edu
MSEC 356, x5924
hours: TR 3-4PM or appt.
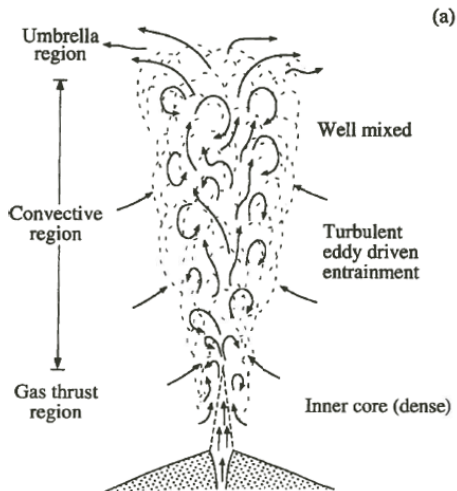
October 07, 2016

(a)

Sparks et al., 1997

Sparks et al., 1997

Density Variations in Eruptive Mix

Density of mixture (β) given by:

$$\frac{1}{\beta} = \frac{1-n}{\sigma} + \frac{n}{\rho}$$

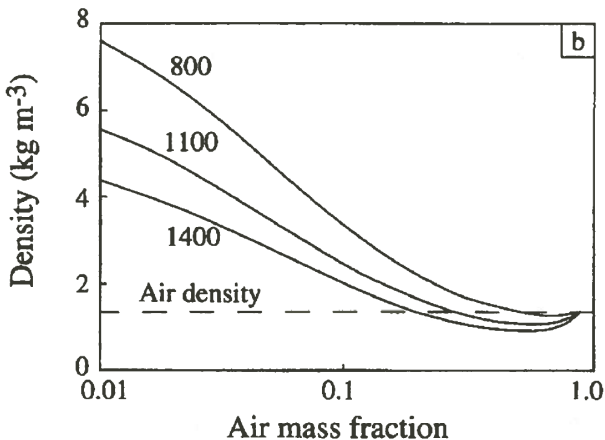n, ρ: mass fraction & density of gas
σ: density of pyroclasts
assume gas phase behaves as perfect gas:

$$\rho = \frac{P}{RT}$$

P, T: pressure & Temperature of mixture
R: gas constant, average if gaseous components: air=285 $Jkg^{-1}K^{-1}$,
$CO_2 = 185 Jkg^{-1}K^{-1}$, water vapor=460$Jkg^{-1}K^{-1}$
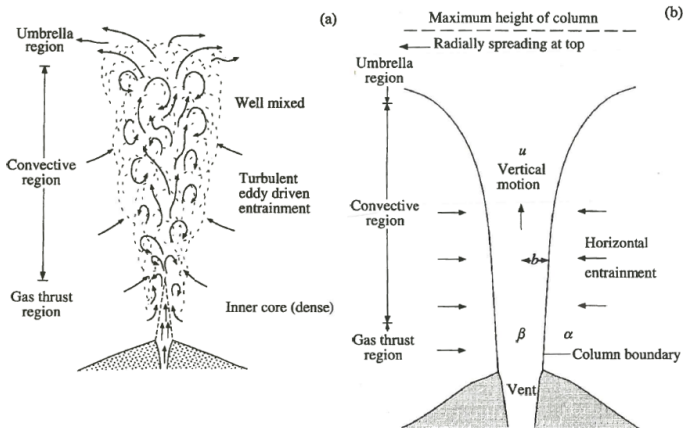
Sparks et al., 1997

Density of mixture (entrained air, pyroclasts, volatiles) function of entrained air; three eruption temperatures given in Kelvin & constant water 3%
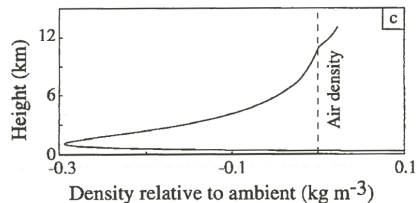
Density Variations in Eruptive Mix

Sparks et al., 1997
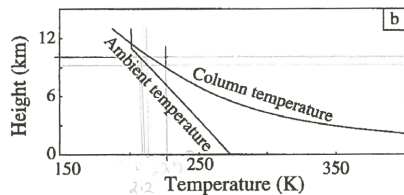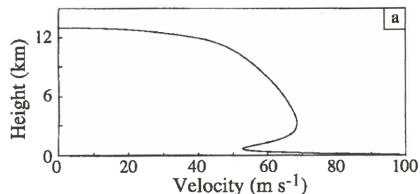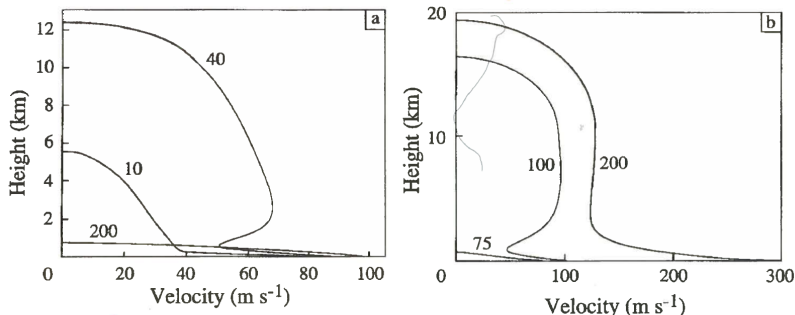
entrainment coefficients: jet $\approx$ 0.06; buoyant plume $\approx$ 0.09 (more efficient; other models exist)

- initial radius: 50 m
- initial velocity: 100 m /s
- eruption temperature: 1000 K
- initial mixtures 3% water (mass fraction)

**Figure 4.5** Variation of the velocity in the column as a function of the height. Curves are shown for (a) three initial radii, 10, 40 and 200 m with eruption velocity of 100 m s^{-1}, and (b) three eruption velocities 200, 100 and 75 m s^{-1} with a radius of 100 m. The mass fraction of water is 0.03 and the eruption temperature 1000 K. With the larger initial radius (a) or smaller eruption velocity (b) the material takes longer to entrain sufficient fluid to become buoyant, eventually leading to collapse in the case of the 200 m initial radius (a) and 75 m s^{-1} initial velocity (b). The 10 m vent radius (a) and 200 m s^{-1} eruption velocity (b) lead to a monotonically decaying velocity profile, since the material becomes buoyant rapidly. However, the 40 m vent radius (a) leads to a non-monotonic velocity profile, because the column entrains ambient air more slowly, and so the velocity falls off dramatically before the material becomes buoyant. A column with this non-linear velocity profile is referred to as superbuoyant. After Bursik and Woods (1991)
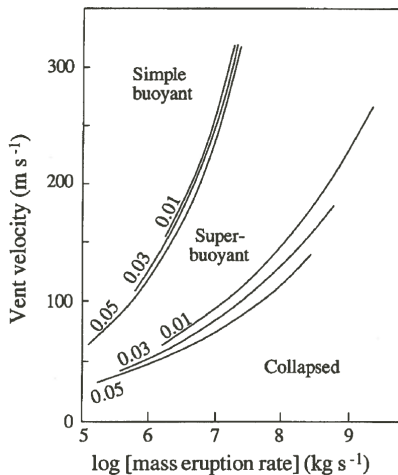
Sparks et al., 1997

Sparks et al., 1997

Solid curves are labeled with initial mass fraction of water
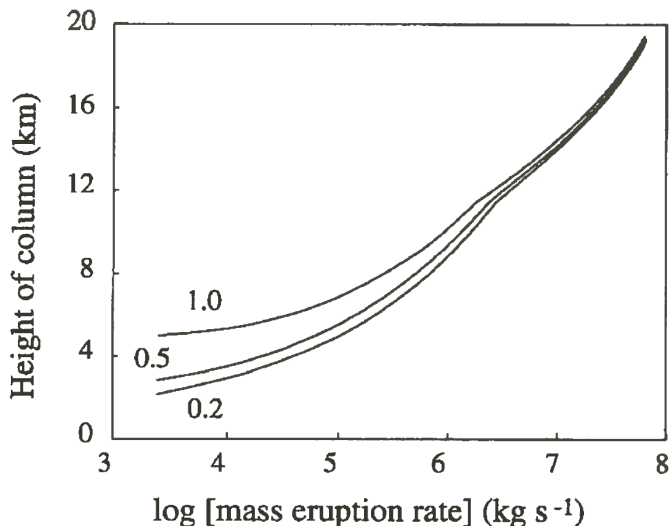
Sparks et al., 1997

Solid curves are labeled with different relative humidities
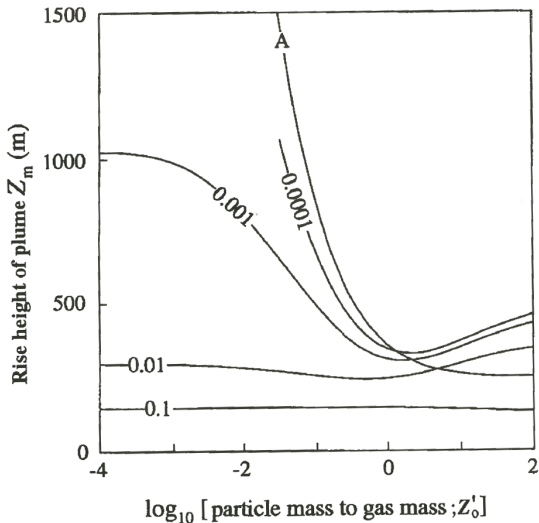
Sparks et al., 1997

10 m vent diameter with 100 m/s initial velocity, curves for different particle radii in meters

board work.
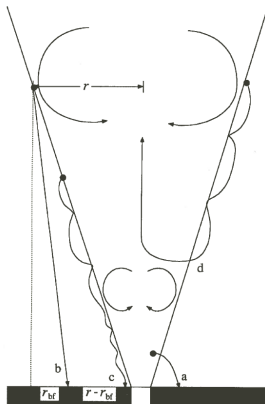
Figure 14.8 Diagram to illustrate sedimentation processes from the margins of a plume or jet. Particles can follow a variety of paths once they fall from a plume, here shown schematically (from Ernst *et al.* 1996a). Particle "a" follows a ballistic path to the ground. Particle "b" hits the ground at a distance, $r - r_{bf}$, that is closer to the plume centreline than is the distance at which it fell from the plume, because of the inward flow of ambient fluid into the plume. The effect of the backflow on particle "c" is sufficiently strong that the particle is almost re-entrained, although the particle is too large to remain in the plume. Particle "d" is simply re-entrained

Sparks et al., 1997

Particle Settling

Form drag - Caused by inertia of air moved from particle path. Force is proportional to projected particle area, $F_i \sim d^2$.

Air Flow

Skin friction - Caused by slowing of air at particle boundary (no-slip condition). Force is proportional to length of path that air parcel must follow around particle, $F_v \sim d$.
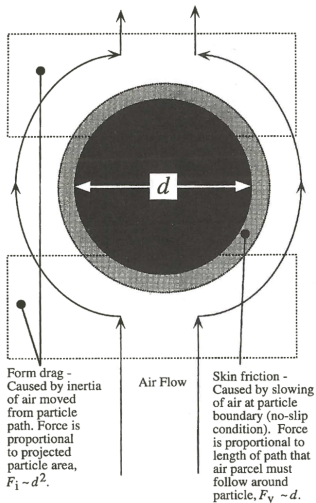
Sparks et al., 1997

Particle Settling

Sparks et al., 1997

Form drag - Caused by inertia of air moved from particle path. Force is proportional to projected particle area, $F_i \sim d^2$.

Air Flow

Skin friction - Caused by slowing of air at particle boundary (no-slip condition). Force is proportional to length of path that air parcel must follow around particle, $F_v \sim d$.
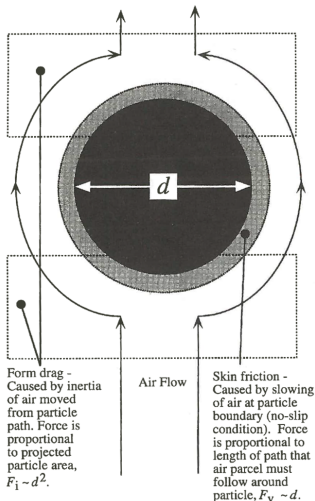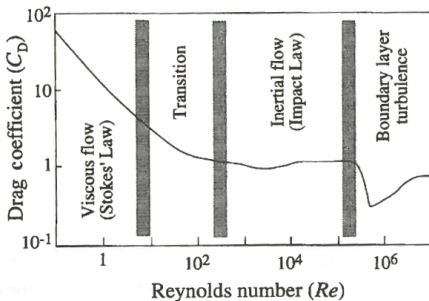
Sparks et al., 1997

- Reynold's number indicates turbidity of flow
- ratio of inertial force (F_i, enhances turbulence) to viscous force (F_v, suppresses turbulence)
- $Re = F_i / F_v = \frac{V_t d}{\nu}$
- d particle diameter, V_t terminal velocity, ν fluid kinematic viscosity (dynamic viscosity / density)

Particle Settling - Terminal Velocity

- Terminal velocity: $V_t = \left(\frac{4}{3} \frac{d(\sigma - \rho)g}{C_d \rho} \right)$
- σ particle density, ρ ambient fluid density (negligible), g acc gravity, C_D drag coeff

Particle Settling - Terminal Velocity

- Terminal velocity: $V_t = \left(\frac{4}{3} \frac{d(\sigma - \rho)g}{C_d \rho} \right)$

- σ particle density, ρ ambient fluid density (negligible), g acc gravity, C_D drag coeff

- particles are irregular, introduce shape factor F to determine drag:

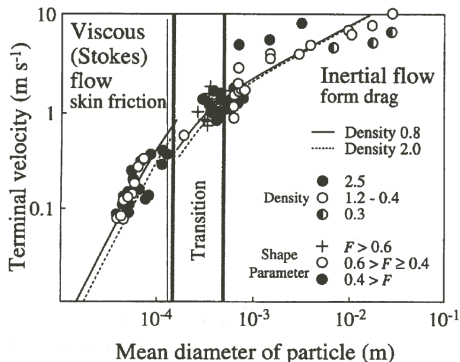- $F = (b_p + c_p)/2a_p$ with $a_p > b_p > c_p$ principal axes of particle

Particle Settling - Terminal Velocity

- Terminal velocity: $V_t = \left(\frac{4}{3} \frac{d(\sigma - \rho)g}{C_d \rho} \right)$

- σ particle density, ρ ambient fluid density (negligible), g acc gravity, C_D drag coeff

- particles are irregular, introduce shape factor F to determine drag:

- $F = (b_p + c_p)/2a_p$ with $a_p > b_p > c_p$ principal axes of particle

- $C_D = \frac{24}{Re} F^{-0.32} + 2\sqrt{1.07 - F}$

Sparks et al., 1997

- Terminal velocity: $V_t = \left(\frac{4}{3} \frac{d(\sigma - \rho)g}{C_d \rho} \right)$
- σ particle density, ρ ambient fluid density (negligible), g acc gravity, C_D drag coeff
- particles are irregular, introduce shape factor F to determine drag:
- $F = (b_p + c_p)/2a_p$ with $a_p > b_p > c_p$ principal axes of particle
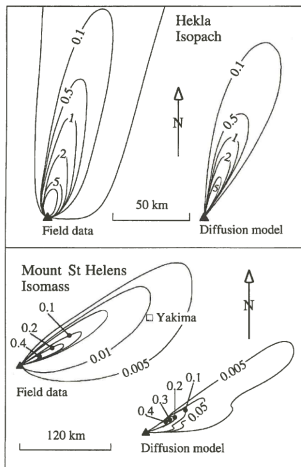- $C_D = \frac{24}{Re} F^{-0.32} + 2\sqrt{1.07 - F}$

Figure 14.15 Predicted deposition patterns compared to isopach data for the August 17, 1980 eruption of Hekla, Iceland, and for the July 22, 1980 eruption of Mount St Helens, Washington, USA. The results from the advection/diffusion modelling are in reasonable agreement with field data for these relatively small eruption plumes (from Glaze and Self 1991)

- allow particles to be advected and dispersed in turbulent wind field, 2nd order PDE

- depends on initial concentration of particles in grain size class,

- depends on eddy diffusivity for atmosphere (non-homogeneous)

- depends on changes in source over time
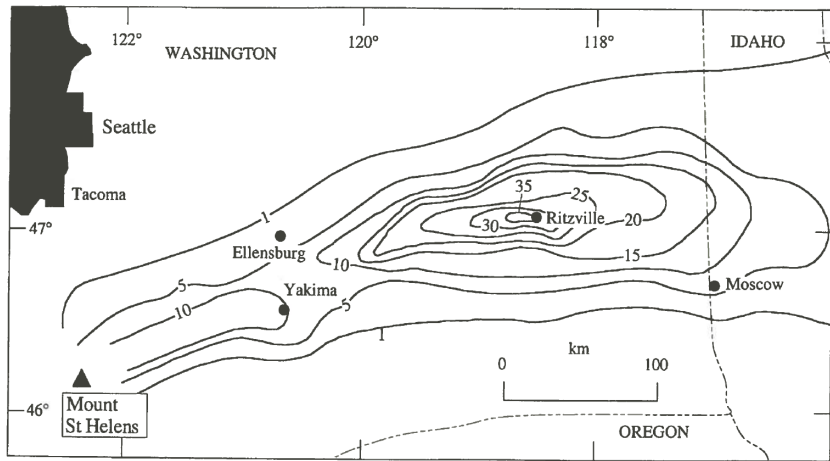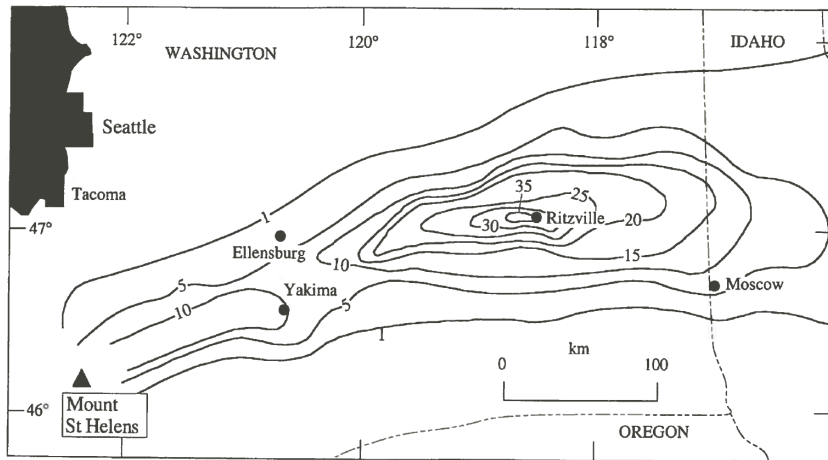
Sparks et al., 1997

Figure 13.12   Isopach map of the Plinian fall deposit from the May 18, 1980 eruption of Mount St Helens, modified from Sarna-Wojcicki *et al.* (1981). A second thickness maximum is present in the vicinity of Ritzville, Washington, and has been attributed to premature settling of fine ash by aggregation. Contours are in millimetres

Sparks et al., 1997

Particle Aggregation

- aggregation of fine ash critical in particle dispersal
- aggregates fall with higher velocity than components (fall out sooner)
- complex grain size distributions
- enhanced thickening of fall deposits
- humidity of plume dictates growth mechanism (dry, accretionary lapilli, mud rain)
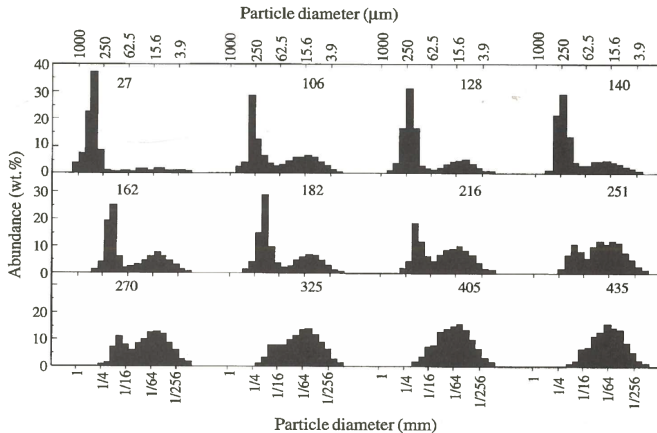
Figure 13.12 Isopach map of the Plinian fall deposit from the May 18, 1980 eruption of Mount St Helens, modified from Sarna-Wojcicki *et al.* (1981). A second thickness maximum is present in the vicinity of Ritzville, Washington, and has been attributed to premature settling of fine ash by aggregation. Contours are in millimetres
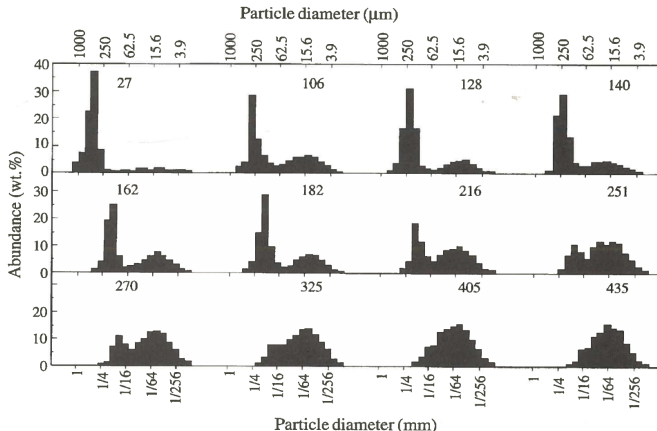
Sparks et al., 1997

Particle Size Distributions

Figure 16.3 Particle size distribution for the bulk deposit of the May 18, 1980 Mount St Helens fall deposit along the dispersal axis. Numbers above histograms are distances, in kilometres, along the dispersal axis. (After Carey and Sigurdsson 1982, reproduced by permission of the American Geophysical Union.)
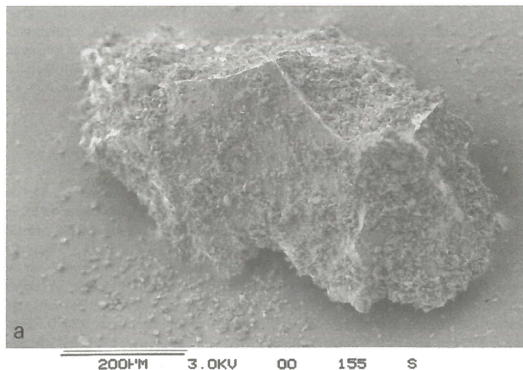
Sparks et al., 1997

Figure 16.3 Particle size distribution for the bulk deposit of the May 18, 1980 Mount St Helens fall deposit along the dispersal axis. Numbers above histograms are distances, in kilometres, along the dispersal axis. (After Carey and Sigurdsson 1982, reproduced by permission of the American Geophysical Union.)

Sparks et al., 1997

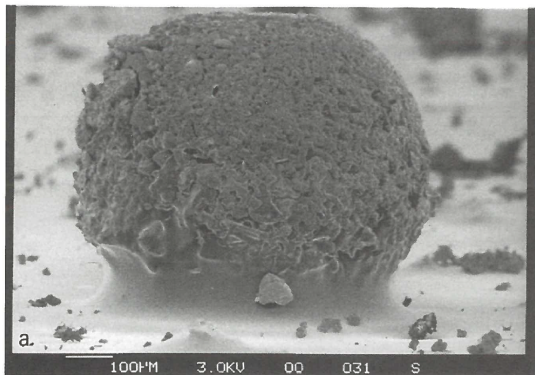polymodal grain size distribution due to deposition of fine material controlled by aggregation

Sparks et al., 1997

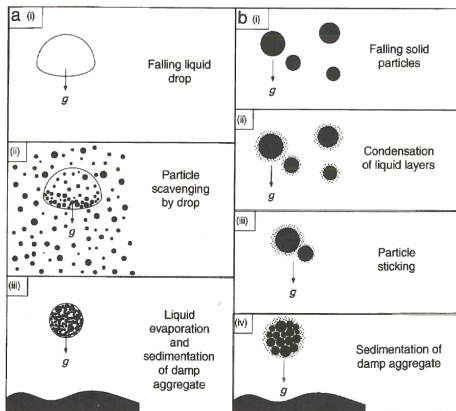Observed at Sakurajima when ground humidity $< 80\%$

Accretionary Lapilli

Sparks et al., 1997

Observed at Sakurajima when ground humidity > 80%
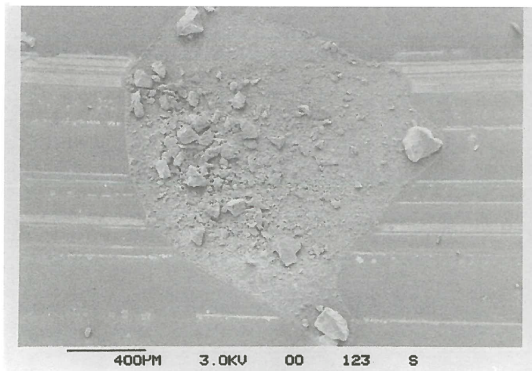
Accretionary Lapilli

Figure 16.12 Hypothesis for the evolution of an accretionary lapillus. (a) A liquid drop falling through a plume scavenges particles and partial evaporation of the drop produces a damp aggregate. (b) Particles in a plume, coated with thin liquid layers, collide and coalesce. (After Gilbert and Lane 1994a, reproduced by permission of *Bulletin of Volcanology*.)

Sparks et al., 1997

Observed at Sakurajima when ground humidity > 80%

Mud Rain

Sparks et al., 1997

Table 16.1 Dominant aggregate collision and binding mechanisms, and physical properties of aggregates

	Dry aggregate	Accretionary lapillus	Mud raindrop
Collision mechanisms			
Ambient plume motions	√	√	√
Fall velocity differences	√	√	√
Electrostatic forces	√		
Binding mechanisms			
Surface tension forces		√	√
Secondary mineral/ice crystal growth		√	
Electrostatic forces	√		
Van der Waals' forces			
Mechanical interlocking			
Physical properties			
Component particle diameter (μm)	< 200	< 90	< 200
Aggregate diameter (mm)	< 5	1–50 (but generally 1–10)	< 5
Density (kg m^{-3})	220–1320	1200–1600	1000–1500
Porosity	0.4–0.9	0.3–0.5 (when dry)	0

Sparks et al., 1997